

5-2013

Reactive Intermediates in Hypoxia-Selective DNA Damage.

Olivia Miller

East Tennessee State University

Follow this and additional works at: <https://dc.etsu.edu/honors>



Part of the [Astrophysics and Astronomy Commons](#)

Recommended Citation

Miller, Olivia, "Reactive Intermediates in Hypoxia-Selective DNA Damage." (2013). *Undergraduate Honors Theses*. Paper 73.
<https://dc.etsu.edu/honors/73>

This Honors Thesis - Open Access is brought to you for free and open access by the Student Works at Digital Commons @ East Tennessee State University. It has been accepted for inclusion in Undergraduate Honors Theses by an authorized administrator of Digital Commons @ East Tennessee State University. For more information, please contact digilib@etsu.edu.

Reactive Intermediates in Hypoxia-Selective DNA Damage

Thesis submitted in partial fulfillment of Honors

By

Olivia Miller
The Honors College
University Honors Scholars Program
Department of Physics and Astronomy
East Tennessee State University

29 April 2013

Yuriy Razskazovskiy, Faculty Mentor

David M. Close, Faculty Reader

Scott Kirkby, Faculty Reader

Abstract

A group of prospective drugs with the aromatic di-N-oxide (ANO) functionality as the common feature are currently undergoing testing for the ability to selectively target tumors surrounded by normal tissues. It has been long recognized that the mechanism of biological activity of these drugs involves DNA damage by free radical species generated through one-electron reduction, although the exact nature of the reactive intermediate responsible for DNA damage remains uncertain. It is believed, however, that one of the key factors defining, in particular, hypoxic selectivity of these drugs is the rate of N-O bond scission in the one-electron reduced intermediate. In this study we have made an attempt to verify whether the predictions made in the literature regarding the N-O bond dissociation rate in a related class of derivatives are applicable to the same process in ANO. For that purpose both theoretical (electronic structure calculations) and experimental (Electron Spin Resonance spectroscopy) have been employed. While our results are not conclusive, they have laid the groundwork for future studies.

1. Introduction

1.1 Aromatic N-oxides (ANO) as prospective anti-cancer drugs

A number of prospective drugs are currently undergoing testing for the ability to selectively target tumors surrounded by normal tissues. A common feature of a large group of these drugs is the aromatic di-N-oxide (ANO) functionality I (Figure 1). The best known representative of this group is tirapazamine II (3-amino-1,2,3-benzotriazine 1,4-dioxide or TPZ Figure 1), which is currently in the final stage of clinical trials before being approved for cancer treatment (Hwang *et al.* 1999).

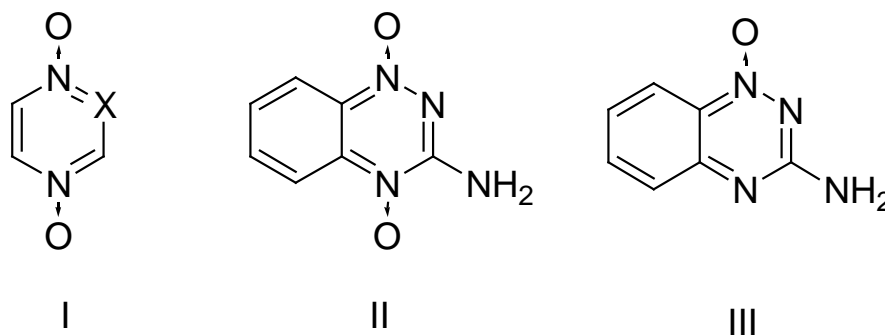


Figure 1. Structures of the di-N-oxide functionality (I), tirapazamine (II) and its metabolite (III)

The principle of selective targeting of solid tumors is based on the fact that the rapid rate of production of tumor cells is known to increase oxygen consumption in tumor tissue (Ramalho *et al.* 2004). Along with this increased oxygen demand, inefficient vascularization results in reduced oxygen distribution to the abnormal tumor tissue (Ramalho *et al.* 2004). Cancer cells in many ways may closely resemble normal cells, but they have poorly oxygenated, or hypoxic, regions. This unique feature of solid tumors makes the difference that can be utilized in cancer treatment (Hwang *et al.* 1999). TPZ, in particular, has shown to be fifteen to two-hundred times

more toxic to oxygen-deficient cells than it is towards normally oxygenated cells in experiments using human and rodent tumor cell lines (Hwang *et al.* 1999). By that criterion TPZ outperforms by far all other compounds of its class, which raises the question of what structural feature makes this compound so special. One of these features is clearly the presence of the di-N-oxide functionality since the product of TPZ metabolism, the corresponding mono-N-oxide III (Figure 1), is not cytotoxic. This observation has led to the conclusion that an intermediate and not the final product in the II \rightarrow III transformation (Figure 1) is responsible for hypoxia-selective cytotoxicity of TPZ and has thus sparked significant attention to the molecular mechanism of this reaction.

1.2 Molecular mechanism of reduction of di-N-oxides into mono-N-oxides

Under biological conditions the di-N-oxide group can undergo one-electron reduction to form a radical-anion IV, which is known to be fairly stable (Birincioglu *et al.* 2003) (Figure 2). This radical anion can act as a base and thus may be protonated to form a neutral radical V in competition with reoxidation with molecular oxygen back into the original inactive form II. Otherwise the protonated intermediate hypothetically undergoes the N-O bond scission, generating a highly damaging hydroxyl radical. Hypoxic selectivity of the drug is determined by competition between the N-O bond scission in the protonated intermediate and the rate of reoxidation of the radical anion by molecular oxygen (Daniels *et al.* 1998).

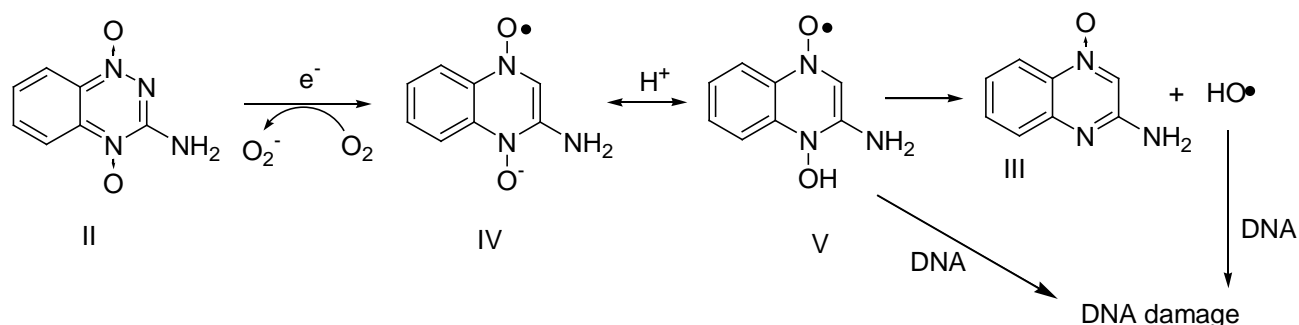


Figure 2. Scheme of the reduction of the di-N-oxide group into a mono-N-oxide group

While there is general agreement that one-electron reduction of TPZ gives rise to a cytotoxic intermediate, the nature of the species responsible for DNA damage remains controversial (Birincioglu *et al.* 2003). It has long been assumed that the neutral radical V causes damage by direct hydrogen abstraction from the DNA backbone (Birincioglu *et al.* 2003). Alternatively it has been suggested that the DNA damage could instead result from the hydroxyl radical released by homolytic N-O bond scission in the activated drug (Ban *et al.* 2001). Neither theory, however, explains how a reactive radical of any kind generated in the bulk, far away from its intended target, can cause DNA damage before being intercepted by other reactive cellular components. Another theory, which eliminates the need for long-distance diffusion of reactive radicals, proposes that TPZ and its metabolites cause radical-mediated cleavage of single-stranded and double-stranded DNA by substituting for molecular oxygen (Hwang *et al.* 1999). In oxygen deficient environments, the effect of radical-based DNA-damaging agents is usually reduced because DNA radicals need to react with molecular oxygen in order to be converted into stable end products such as strand breaks (Daniels *et al.* 1998). Experiments have revealed that TPZ and its metabolites can act as a surrogate for molecular oxygen by both initiating the formation of DNA radicals and reacting with the DNA radicals, resulting in oxygenation of the radical sites (Birincioglu *et al.* 2003). It is believed that these reactions generate an intermediate VI, which is a close analog of the protonated radical anion V (Figure 3).

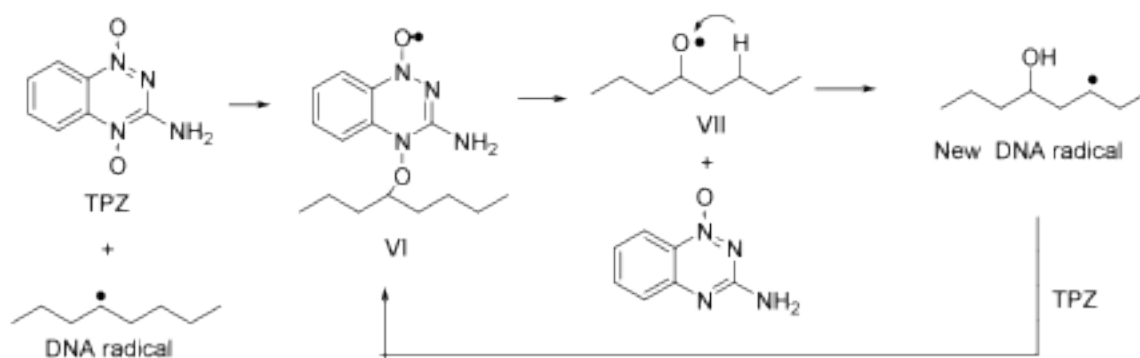


Figure 3. Formation of and reaction with DNA radicals by TPZ and its metabolites

The N-O bond scission in this intermediate would generate a DNA alkoxy radical VII, whose reactivity is similar to that of hydroxyl radicals. Further hydrogen abstraction by this radical from a neighboring site with subsequent oxidation by TPZ may lead to a chain DNA oxidation and therefore amplification of DNA damage by the drug. This mechanism, in particular, emphasizes the potential significance of N-O bond scission for the biological activity of aromatic N-oxides.

1.3 Rates of N-O bond scission in one-electron reduced N-oxides

Despite the uncertainty in the exact nature of DNA damage by the reactive intermediate, it is known that the rate of the N-O bond scission plays a significant role in the hypoxic selectivity of the antitumor compound. The ability of the one-electron reduced antitumor compound to generate a cytotoxic species depends on the efficiency of the irreversible N-O bond fragmentation as compared to the probability the radical intermediate is reoxidized to return to the original inactive form of the drug. Direct experimental data on the rates of N-O bond scission in protonated radical anions of aromatic di-N-oxides are unavailable. There is information, however, on the rate of this process in structurally related radicals generated by one-electron reduction of N-methoxypyridinium cations VIII, and theoretical investigation of this process has been performed for the one-electron reduced N-hydroxypyrazinium model compound IX (Figure 4) (Lorance *et al.* 2002).

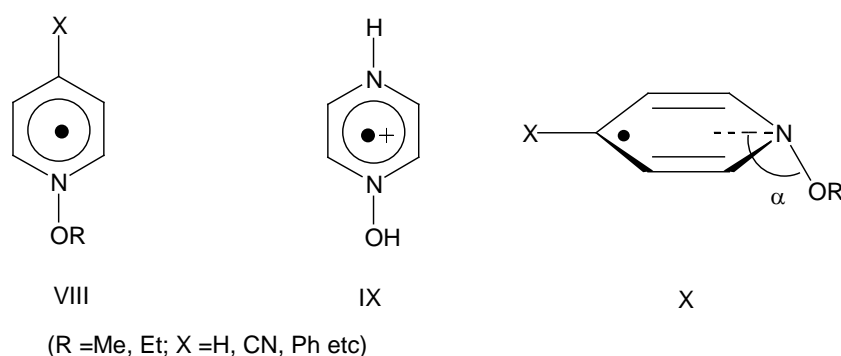


Figure 4. Structures of N-methoxypyridinium cation (VIII), N-hydroxypyrazinium compound (IX), and radical VIII with angle α formed by N-OR bond and plane of the ring structure (X)

It has been concluded, in particular that the rate of N-O bond scission in VIII correlates with the extent of non-planarity of its structure, which can be characterized by angle α formed by the N-OR bond with the plane of the ring (Lorance *et al.* 2002). In a perfectly planar geometry ($\alpha = 180^\circ$) the ground state of the radical (which is a π^* state by the nature of the singly occupied molecular orbital) correlates not with the ground state of the products (which is a σ -state by its orbital origin) but with an $n\pi^*$ -excited state of the aromatic heterocycle formed after N-O bond scission. The electronic state of the radical that correlates directly with the ground state of the products is its first excited σ^* -state (Figure 5).

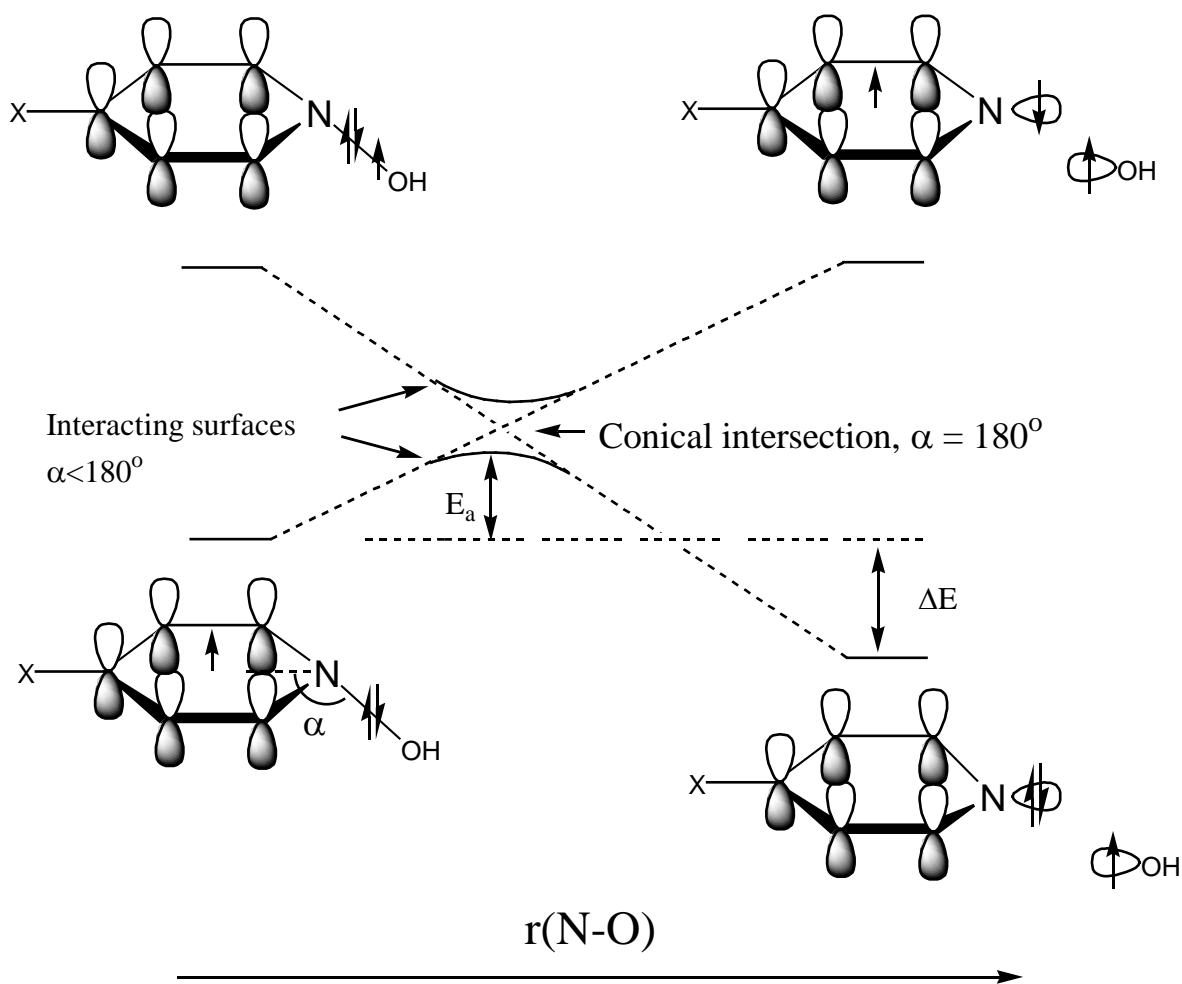


Figure 5. Excited and ground state potential energy surfaces of N-O bond fragmentation where interaction of the surfaces occurs at the conical intersection, $\alpha = 180^\circ$

In the planar structure the π^* and σ^* states do not interact since they have different symmetries (A'' and A' in the C_s point group). Without the plane of symmetry, as in the case of $\alpha \neq 180^\circ$, this restriction is absent and the potential energy surfaces can interact as shown by solid lines in Figure 5. As a result, the two potential energy surfaces intersect at a single point with generalized coordinates $\alpha = 180^\circ$ and some value of r_{N-O} . This situation is termed a “conical intersection” since in three dimensions with the energy of the system plotted as the function of r_{N-O} and α the potential energy surfaces resemble two cones (one upside down) sharing the same vertex (Lorance *et al.* 2002).

Higher activation energies, E_a , resulting into slower reaction rates are generally expected for those processes whose transition states lie close to conical intersections. For the intermediates of interest, the transition state geometry has been correlated with the equilibrium bending angle α in the ground state of the radical (Lorance *et al.* 2002). Thus the less planar the equilibrium geometry is, the farther the reaction transition state is from conical intersection, and the faster is the N-O bond fragmentation. The flattest radical VIII (X=1-methylpyridinium-4-yl) with an angle of $\alpha = 175^\circ$ had the slowest reaction rate of $k_{fr} = 4.0 \times 10^4 \text{ s}^{-1}$ while the most bent radical (X = Ph) with an angle of $\alpha = 148^\circ$ had the fastest reaction rate of $k_{fr} = 2.7 \times 10^{11} \text{ s}^{-1}$ (Lorance *et al.* 2002).

Another experimental and theoretical finding is that the presence of an electron-withdrawing group X in radical VIII may slow down the rate of N-O bond fragmentation. Theoretical analysis has shown that the presence of an electron-withdrawing substituent stabilizes the π^* -ground state of the radical causing its geometry to be flatter, thereby making the transition-state geometry closer to that of a conical intersection that increases the activation energy E_a (Lorance *et al.* 2002). Second, the increased electron affinity of the radical makes its

dissociation less energetically favorable (smaller ΔE in Figure 6) as follows from a thermochemical cycle shown below (Figure 6).

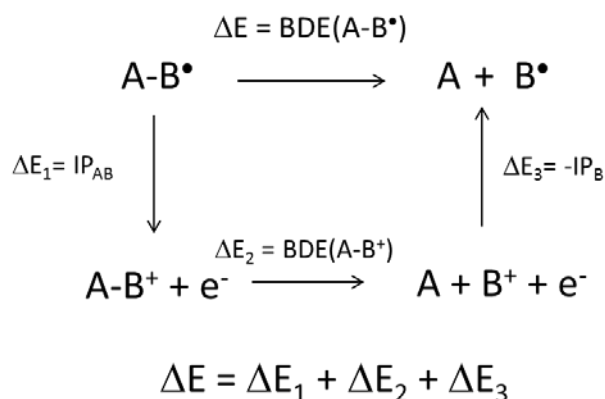


Figure 6. Thermochemical cycle of bond dissociation in radical A-B

In this cycle electron-withdrawing substituents increase the ionization potential, IP, of the radical (ΔE_1) while N-O bond dissociation energy BDE (ΔE_2) in the cation produced by ionization and electron affinity of the dissociation product B^+ (ΔE_3) are practically unaffected. The expected result is an overall increase in ΔE mostly due to the contribution from ΔE_1 . Since activation energies for reactions of the same type are typically reduced with the increase in the reaction energetics, radicals VIII with weaker electron-withdrawing substituents X should undergo fragmentation faster than those with stronger electron-withdrawing substituents. For example, when X = Ph, a relatively weak electron-withdrawing group, $k_{fr} = 2.7 \times 10^{11} \text{ s}^{-1}$, and when X = NC, a strong-electron-withdrawing group, $k_{fr} = 1.2 \times 10^{10} \text{ s}^{-1}$.

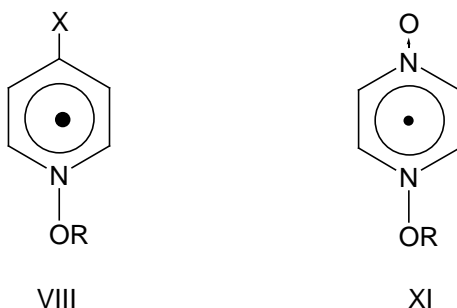


Figure 7. Structures of N-methoxy radical (VIII) and one-electron reduced di-N-oxide (XI)

Given that the second N-oxide group in the para-position to the N-OR bond acts as a strong electron-withdrawing substituent, the implications are that one-electron reduced di-N-oxides XI (Figure 7) must be:

- a) more planar compared to derivatives VIII in terms of the N-O bending angle:
- b) more stable in terms of the dissociation energies ΔE , and
- c) have a higher dissociation activation energy E_a than the corresponding mono-N-oxide derivatives.

Verification of these predictions is the goal of the present project.

2. Objectives

2.1. *To compare molecular geometries and electronic structures of protonated radical anions of aromatic mono- and di-N-oxides*

By comparing the molecular geometries, we plan to establish whether the N-O out-of-plane bending angle is substantially different in radicals with general structure VIII and XI (Figure 7). Another goal is to establish the spin density distribution in both kinds of the species for further comparison with Electron Spin Resonance (ESR) data.

2.2 *To compare the activation and N-O bond dissociation energies in protonated radical anions of aromatic mono- and di-N-oxides*

The goal of this study is to verify the prediction that an N-oxide moiety in the para-position to the N-OH bond increases E_a and decreases ΔE compared to the structures without this functionality. If confirmed, this would mean that the di-N-oxide derivatives are more stable towards the N-O bond scission than the corresponding mono-N-oxide derivatives.

2.3 To compare theoretically predicted spin density distributions in protonated radical anions of aromatic di-N-oxides with those found experimentally by means of Electron Spin Resonance (ESR) spectroscopy.

The results of this part of the study will give us some independent verification of how accurate and reliable are the theoretical methods employed in the first two paragraphs of this section.

3. Methods

3.1 Computational techniques

All electronic structures were calculated by numerically solving the Schrodinger equation using the unrestricted Hartree-Fock (UHF) formalism and the Molecular Orbitals as Linear Combination of Atomic Orbitals (MO-LCAO) theoretical model. The atomic orbitals were approximated by a 6-31G(d) set of model Gaussian functions. The calculations were performed using a Gaussian 03 suite of programs. Full geometry optimization was performed to determine the equilibrium geometries of the model structures representing protonated radical anions of pyrazine-1,4-dioxide (X) and pyrazine-1-oxide (XI).

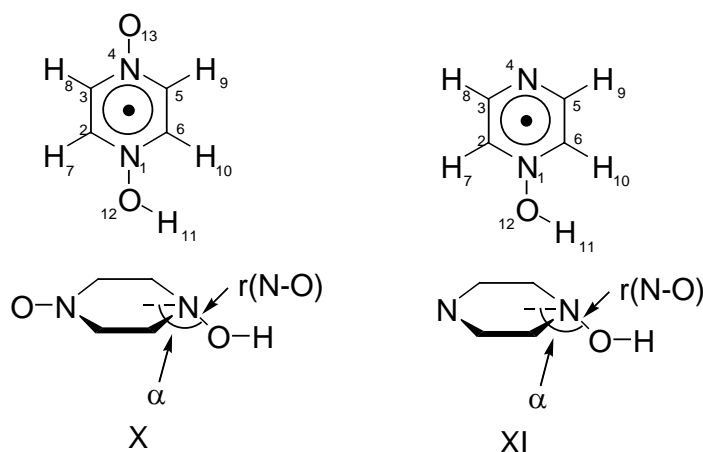


Figure 8. Model structures of protonated radical anions of pyrazine-1,4-dioxide (X) and pyrazine-1-oxide (XI)

To determine the activation energy for N-O bond dissociation in both radicals the corresponding transition state structure was located through a reaction path calculation. The N-O bond length was chosen as the “pseudo reaction coordinate”, and twenty-one points were geometry-optimized at different values of the N-O bond length $r_{\text{N-O}}$ (from about 1.4 to 1.79 Å at .02 Å intervals). The points at the different values of $r_{\text{N-O}}$ were used to construct an electronic energy profile. The transition state of each structure, which is a maximum along the reaction path, was calculated separately specifically using a transition state (TS) optimization. The transition state is characterized by an imaginary vibrational frequency corresponding to the stretching of the N-O bond moving towards the reactants in one direction and towards the products in the other.

The final state of the system is the state in which the nitrogen and oxygen bond length is considered to be infinitely large. To determine the energy of this dissociated state for both structures, the hydroxyl group of radicals X and XI were placed at a fixed 5.00 Å distance from the aromatic ring, and the dissociated structures were geometry-optimized. We compared the energy of the dissociated state to that of the initial state for both structures to determine the total energy of the reaction, ΔE , where $\Delta E = E_{\text{final}} - E_{\text{initial}}$.

3.2 Electron Spin Resonance

In order to experimentally verify the accuracy of the theoretically predicted spin density distribution in protonated radical anions of aromatic di-N-oxides, we used Electron Spin Resonance (ESR) spectroscopy. ESR is a resonance absorption of electromagnetic radiation by a system with a non-zero electronic spin placed in an external magnetic field. Energy levels of a free radical ($S = 1/2$) placed into external magnetic field \mathbf{H} and interacting with n nuclei having nuclear spins \mathbf{I}_i are given by the spin-Hamiltonian:

$$H = \beta HgS + \sum_{i=1}^n a_i S I_i + \sum_{i=1}^n S T_i I_i$$

where β is the Bohr magneton, g is the g -tensor of the radical, a_i and T_i are isotropic (Fermi-contact) hyperfine coupling constants and dipole-dipole coupling tensors with the i -th nucleus, respectively. The latter two parameters are available from the electronic structure calculations described above, and, therefore, direct comparison of predicted and experimental values can be performed. The free radical species XIII and XV studied experimentally are shown in Figure 9.

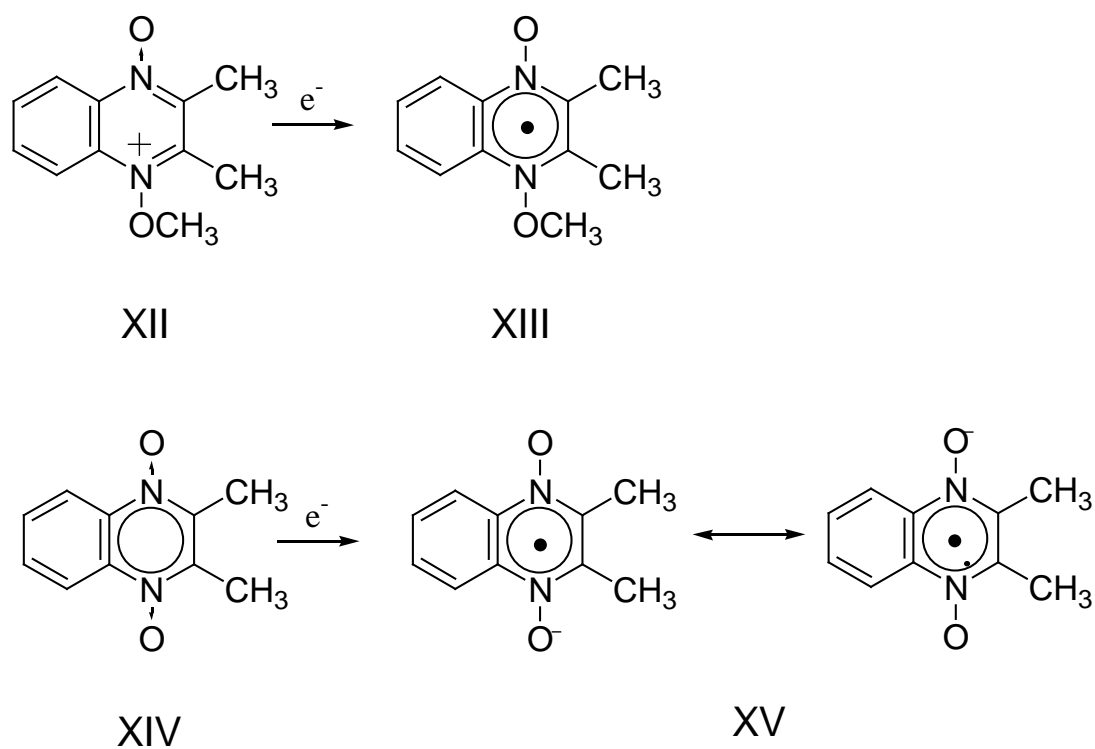


Figure 9. Structures of precursors 1-methoxy-2,3-dimethyl(quinoxalinium)-4-oxide (XII) and 2,3-dimethylquinoxaline-1,4-dioxide (XIV) and their corresponding free radical species (XIII and XV, respectively)

Both were generated by free electron attachment to the corresponding precursors 1-methoxy-2,3-dimethyl(quinoxalinium)-4-oxide XII (0.084 M) and 2,3-dimethylquinoxaline-1,4-dioxide XIV (c.a. 0.1 M) dissolved in 5M aqueous lithium chloride solution, which forms a glass upon freezing at 77 K. The choice of precursors was determined primarily by their sufficiently high

solubility in 5M LiCl. Free electrons were generated through ionization of the matrix by X-irradiation at 77 K, and all subsequent manipulations with the samples were performed at this temperature. The electron-loss centers generated by irradiation are trapped in the matrix as dichloride radical anions Cl_2^- , which are also paramagnetic. As a result, the ESR spectra obtained by irradiation contained the signatures of both electron attachment products and Cl_2^- . The spectrum of the latter was further subtracted to reveal the ESR signature of one-electron reduced intermediates. The benchmark spectrum of Cl_2^- needed for this purpose was generated by X-irradiation of a dilute solution of gaseous chlorine in 5M LiCl, which forms Cl_2^- as the only irradiation paramagnetic product. First-derivative ESR spectra were taken using an X-band (9 GHz) ESR spectrometer (100 kHz field modulation) operated at 2 mW of microwave power to avoid saturation of the signal.

4. Results

4.1 Electronic Structure Calculations

Table 1 below contains the computational results of the equilibrium geometries and the spin density distributions of the protonated radical anions X and XI. The equilibrium geometries included in the table are those directly involved in the N-O bond fragmentation: the N-O bond length, $r_{\text{N-O}}$ (Å), and the dihedral angle (degrees) that characterizes the N-O out of plane bending. The spin density distributions in the table include the isotropic (Fermi-contact) coupling constants and the T-tensor principal values for nitrogen in the 1 and 4-positions of the structures. The hyperfine interactions with the aromatic hydrogens in the 2, 3, 5 and 6-positions are not included since these nuclei are missing in the experimentally studied intermediates.

Table 1. Equilibrium geometries and spin density distribution in protonated radical anions of pyrazine-1,4-dioxide (X) and pyrazine-1-oxide (XI)

Structure	X			XI		
Equilibrium geometry						
r(N-O), Å	1.39			1.38		
Dihedral angle, degrees	135.5			146.5		
Isotropic (Fermi contact) coupling constants <i>a</i>, Gauss						
N1	9.323			17.303		
N4	19.355			21.884		
T-tensor principal values, Gauss						
	xx	yy	zz	xx	yy	zz
N1	-2.695	-1.600	4.294	-4.702	-3.819	8.521
N4	-6.849	-6.689	13.538	-9.071	-8.982	18.052

4.2 Reaction path calculations

Figures 10 and 11 below represent the reaction path of the N-O bond dissociation of radicals X and XI, respectively. Each of the twenty-one points along the path represent the energy (kJ/mol) at a specific value of the N-O bond length $r_{\text{N-O}}$ (Å). The maximum along the reaction path represents the transition state of each structure, which corresponds to the activation energy, E_a , of the N-O bond dissociation. The dissociated state for both structures is located at 5.00 Å. Table 2 summarizes the energetics of N-O bond dissociation for both radicals.

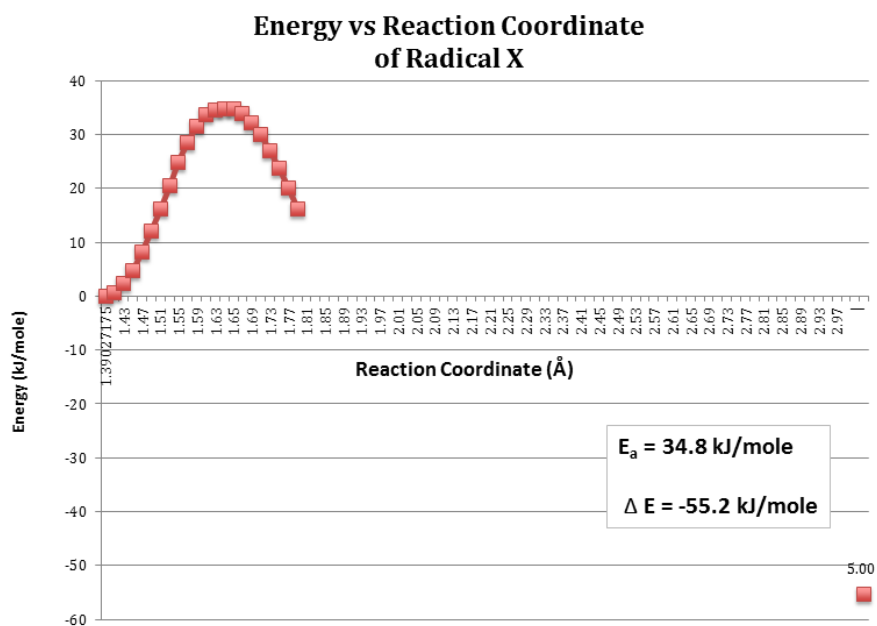


Figure 10

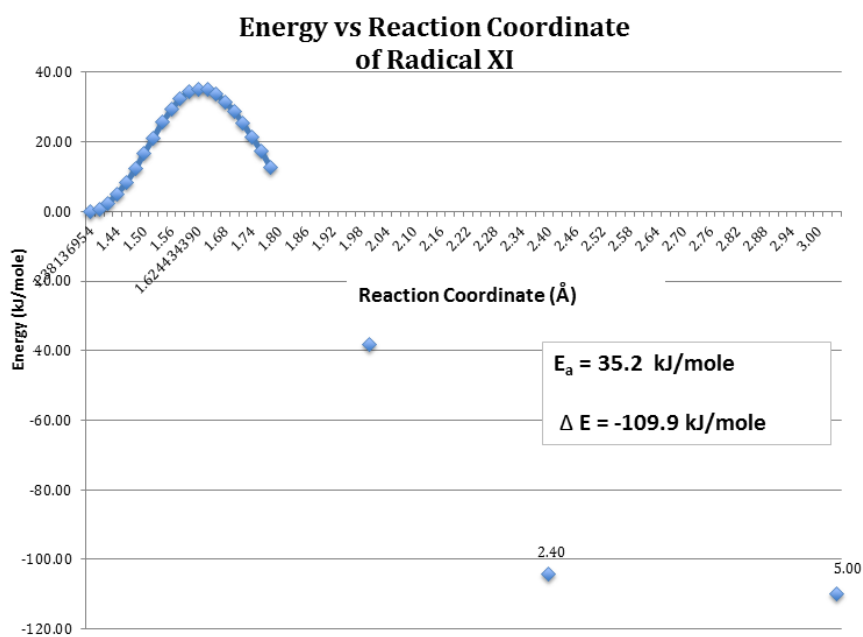


Figure 11

Table 2. Summary on the N-O bond dissociation energetics

Structure	X	XI
E_a , kJ/mol	34.8	35.2
ΔE , kJ/mol	-55.3	-109.9

4.3 ESR data

Figure 12 below displays the ESR spectra results in units of Gauss. The solid spectra lines in Figures 12A and 12B are the spectra of the electron attachment products of radicals XIII and XV, respectively, when dissolved in a 5M lithium chloride solution while the dashed line represents the spectrum of Cl_2^- . In Figures 12C and 12D the benchmark spectrum of Cl_2^- has been subtracted in order to display the spectra results of only the respective electron reduced intermediates XIII and XV.

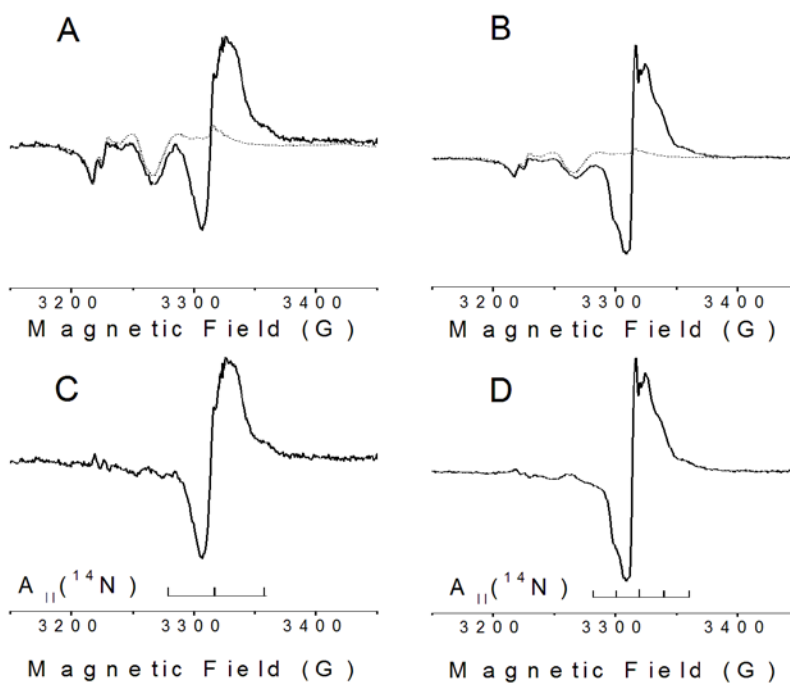


Figure 12. ESR spectra results

5. Discussion

5.1 *Equilibrium geometries of free radical species X and XI*

It has been previously suggested by Lorance *et al.* that introduction of an electron-withdrawing group into para-position to the N-OH bond tends to make the structure more planar (Lorance *et al.* 2002). Our results show, however, that the angle α between the N-OH bond and the plane of the ring for is smaller in radical X than in radical XI while the N-OH bond lengths in both species are practically the same. The smaller angle contradicts the expectation based on the literature data cited above since the N-oxide moiety is known to possess strong electron withdrawing properties. It may therefore be concluded that electron affinity of the para-substituent is likely not the only factor controlling geometry of the intermediates.

5.2 *Energetics of the N-OH bond dissociation and thermal stability*

In calculating the energetics of dissociation for the intermediates, we found that the N-O bond dissociation energy in X is about half that of XI. This result is consistent with the prediction that the addition of a strong electron-withdrawing substituent, which increases the ionization potential of the radical, makes the process of dissociation of the N-OH bond less energetically favorable. At the same time, the activation energies of dissociation E_a affecting the rates of the N-OH bond rupture were found to be about the same for both of the structures. Our results, therefore, do not predict a substantial difference in thermal stability of radicals X and XI with respect to unimolecular dissociation. In general this prediction disagrees with the common qualitative rule that more energetically favorable processes typically proceed with lower activation energies. The apparent violation of this rule in the present case may be a result of the involvement of two factors affecting E_a in opposite directions: the smaller energetics of

dissociation of radical X, which tends to increase E_a , and the more bent structure of this intermediate that moves the transition state away from the conical intersection, thereby decreasing E_a .

5.3 Theoretical and ESR spin density distributions

According to the theoretical model calculations, substantial hyperfine coupling (both isotropic and dipole-dipole) in radicals X and XI should be expected with both of the heterocyclic nitrogens. Hyperfine interactions with the aromatic hydrogens in the 2, 3, 5 and 6-positions are also substantial but not discussed since these nuclei are missing in the experimentally studied intermediates (Figure 8). Direct comparison of experimental and theoretical hyperfine coupling parameters can be partially performed for radical XIII, whose ESR spectrum is shown in Figure 12C. The large width and poor resolution of the spectrum indicate multiple unresolved hyperfine interactions with multiple nuclei. The two shoulder-like features on the wings may be associated with the largest predicted hyperfine coupling that involves N4 ($I = 1$). If so, a pattern of three equally spaced lines separated by a distance of $A_{II} = a + T_{zz} \approx 33$ G should be expected. The experimental width of this spectrum is about 75 Gauss that is reasonably close to the predicted value of $2A_{II} = 66$ G.

To verify that this spectrum is indeed a result of coupling with a nitrogen atom in XIII, we compared it to the spectrum of radical anion XV, where the spin density is shared between two nitrogen atoms, that reduces all hyperfine coupling parameters by a factor of two. The hyperfine pattern produced by two equivalent nitrogens consists of five equally spaced lines separated by a distance $A_{II}' = \frac{1}{2} A_{II} \approx 16.5$ G but has an overall spectrum width that is the same as when the coupling is with a single nitrogen atom. In keeping with this expectation, the ESR spectrum of radical XV, as shown in Figure 12D, indeed has two additional hyperfine features

and the total width of about 75 Gauss that is consistent with the prediction made above. Thus the theoretical spin density distributions are generally consistent with our experimental results, confirming the reliability of the theoretical methods employed in electronic structure calculations.

6. Conclusions

The theoretical and experimental results concerning protonated radical anions of aromatic mono- and di-N-oxides are not conclusive. Although dissociation of the model radical X was found to be less exoergic than for the corresponding mono-N-oxide derivative XI, the activation energy of its dissociation does not seem to be greater, thus predicting a similar thermal stability. In agreement with theoretical predictions, the ESR spectra of radical XIII show features that can tentatively be assigned to anisotropic hyperfine interactions with one ^{14}N nucleus ($I = 1$). However, poor resolution in the spectrum does not allow for more detailed analysis of the hyperfine interactions. More conclusive results could possibly be obtained by using an isotopically substituted derivative containing ^{15}N ($I = 1/2$) instead of ^{14}N , but the precursors required for this study are not available at present.

REFERENCES

- Ban, F., Gauld, J. W., & Boyd, R. J. (2001). Modeling the action of antitumor drug: A density functional theory study of the mechanism of tirapazamine. *J. Am. Chem. Soc.* *123*(30), 7320-7325.
- Birincioglu, M., Jaruga, P., Chowdhury, G., Rodriguez, H., Dizdaroglu, M., & Gates, K. S. (2003). DNA base damage by the antitumor agent 3-amino-1,2,4-benzotriazine 1,4-dioxide (tirapazamine). *J. Am. Chem. Soc.* *125*(38), 11607-11615.
- Daniels, J. S., Gates, K. S., Tronche, C., & Greenberg, M. M. (1998). Direct evidence for bimodal DNA damage induced by tirapazamine. *Chem. Res. Toxicol.* *11*(11), 1254-1257.
- Hwang, J., Greenberg, M. M., Fuchs, T., & Gates, K. S. (1999). Reaction of the hypoxia-selective antitumor agent tirapazamine with a C1'-radical in single stranded and double-stranded dna: The drug and its metabolites can serve as surrogates for molecular oxygen in radical-mediated DNA damage reactions. *Bio. Chem.* *38*(43), 14248-14255.
- Lorance, E. D., Wolfgang, K. H., & Gould, I. R. (2002). Kinetics of reductive n-o bond fragmentation: The role of a conical intersection. *J. Am. Chem. Soc.* *124*(51), 15225-15238.
- Ramalho, T. C., Da Cunha, E. F. F., & De Alencastro, R. B. (2004). Theoretical study of adiabatic and vertical electron affinity of radiosensitizers in solution part 2: analogues of tirapazamine. *J. Theor. Comput. Chem.* *3*(1), 1-13.